

Improved Measurement of the Evolution of the Reactor Antineutrino Flux and Spectrum at Daya Bay

F. P. An,¹ W. D. Bai,¹ A. B. Balantekin,² M. Bishai,³ S. Blyth,⁴ G. F. Cao,⁵ J. Cao,⁵ J. F. Chang,⁵ Y. Chang,⁶ H. S. Chen,⁵ H. Y. Chen,⁷ S. M. Chen,⁷ Y. Chen,^{8,1} Y. X. Chen,⁹ J. Cheng,⁹ J. Cheng,⁹ Y.-C. Cheng,⁴ Z. K. Cheng,¹ J. J. Cherwinka,² M. C. Chu,¹⁰ J. P. Cummings,¹¹ O. Dalager,¹² F. S. Deng,¹³ Y. Y. Ding,⁵ M. V. Diwan,³ T. Dohnal,¹⁴ D. Dolzhikov,¹⁵ J. Dove,¹⁶ K. V. Dugas,¹² H. Y. Duyang,¹⁷ D. A. Dwyer,¹⁸ J. P. Gallo,¹⁹ M. Gonchar,¹⁵ G. H. Gong,⁷ H. Gong,⁷ W. Q. Gu,³ J. Y. Guo,¹ L. Guo,⁷ X. H. Guo,²⁰ Y. H. Guo,²¹ Z. Guo,⁷ R. W. Hackenburg,³ Y. Han,¹ S. Hans,^{3,*} M. He,⁵ K. M. Heeger,²² Y. K. Heng,⁵ Y. K. Hor,¹ Y. B. Hsiung,⁴ B. Z. Hu,⁴ J. R. Hu,⁵ T. Hu,⁵ Z. J. Hu,¹ H. X. Huang,²³ J. H. Huang,⁵ X. T. Huang,¹⁷ Y. B. Huang,²⁴ P. Huber,²⁵ D. E. Jaffe,³ K. L. Jen,²⁶ X. L. Ji,⁵ X. P. Ji,³ R. A. Johnson,²⁷ D. Jones,²⁸ L. Kang,²⁹ S. H. Kettell,³ S. Kohn,³⁰ M. Kramer,^{18,30} T. J. Langford,²² J. Lee,¹⁸ J. H. C. Lee,³¹ R. T. Lei,²⁹ R. Leitner,¹⁴ J. K. C. Leung,³¹ F. Li,⁵ H. L. Li,⁵ J. J. Li,⁷ Q. J. Li,⁵ R. H. Li,⁵ S. Li,²⁹ S. C. Li,²⁵ W. D. Li,⁵ X. N. Li,⁵ X. Q. Li,³² Y. F. Li,⁵ Z. B. Li,¹ H. Liang,¹³ C. J. Lin,¹⁸ G. L. Lin,²⁶ S. Lin,²⁹ J. J. Ling,¹ J. M. Link,²⁵ L. Littenberg,³ B. R. Littlejohn,¹⁹ J. C. Liu,⁵ J. L. Liu,³³ J. X. Liu,⁵ C. Lu,³⁴ H. Q. Lu,⁵ K. B. Luk,^{30,18,35} B. Z. Ma,¹⁷ X. B. Ma,⁹ X. Y. Ma,⁵ Y. Q. Ma,⁵ R. C. Mandujano,¹² C. Marshall,^{18,†} K. T. McDonald,³⁴ R. D. McKeown,^{36,37} Y. Meng,³³ J. Napolitano,²⁸ D. Naumov,¹⁵ E. Naumova,¹⁵ T. M. T. Nguyen,²⁶ J. P. Ochoa-Ricoux,¹² A. Olshevskiy,¹⁵ J. Park,²⁵ S. Patton,¹⁸ J. C. Peng,¹⁶ C. S. J. Pun,³¹ F. Z. Qi,⁵ M. Qi,³⁸ X. Qian,³ N. Raper,¹ J. Ren,²³ C. Morales Revecó,¹² R. Rosero,³ B. Roskovec,¹⁴ X. C. Ruan,²³ B. Russell,¹⁸ H. Steiner,^{30,18} J. L. Sun,³⁹ T. Tmej,¹⁴ K. Treskov,¹⁵ W.-H. Tse,¹⁰ C. E. Tull,¹⁸ Y. C. Tung,⁴ B. Viren,³ V. Vorobel,¹⁴ C. H. Wang,⁶ J. Wang,¹ M. Wang,¹⁷ N. Y. Wang,²⁰ R. G. Wang,⁵ W. Wang,^{1,37} X. Wang,⁴⁰ Y. Wang,³⁸ Y. F. Wang,⁵ Z. Wang,⁵ Z. Wang,⁷ Z. M. Wang,⁵ H. Y. Wei,^{3,‡} L. H. Wei,⁵ L. J. Wen,⁵ K. Whisnant,⁴¹ C. G. White,¹⁹ H. L. H. Wong,^{30,18} E. Worcester,³ D. R. Wu,⁵ Q. Wu,¹⁷ W. J. Wu,⁵ D. M. Xia,⁴² Z. Q. Xie,⁵ Z. Z. Xing,⁵ H. K. Xu,⁵ J. L. Xu,⁵ T. Xu,⁷ T. Xue,⁷ C. G. Yang,⁵ L. Yang,²⁹ Y. Z. Yang,⁷ H. F. Yao,⁵ M. Ye,⁵ M. Yeh,³ B. L. Young,⁴¹ H. Z. Yu,¹ Z. Y. Yu,⁵ B. B. Yue,¹ V. Zavadskiy,^{3,15} S. Zeng,⁵ Y. Zeng,¹ L. Zhan,⁵ C. Zhang,³ F. Y. Zhang,³³ H. H. Zhang,¹ J. L. Zhang,³⁸ J. W. Zhang,⁵ Q. M. Zhang,²¹ S. Q. Zhang,¹ X. T. Zhang,⁵ Y. M. Zhang,¹ Y. X. Zhang,³⁹ Y. Y. Zhang,³³ Z. J. Zhang,²⁹ Z. P. Zhang,¹³ Z. Y. Zhang,⁵ J. Zhao,⁵ R. Z. Zhao,⁵ L. Zhou,⁵ H. L. Zhuang,⁵ and J. H. Zou⁵

(The Daya Bay Collaboration)

¹*Sun Yat-Sen (Zhongshan) University, Guangzhou*

²*University of Wisconsin, Madison, Wisconsin 53706*

³*Brookhaven National Laboratory, Upton, New York 11973*

⁴*Department of Physics, National Taiwan University, Taipei*

⁵*Institute of High Energy Physics, Beijing*

⁶*National United University, Miao-Li*

⁷*Department of Engineering Physics, Tsinghua University, Beijing*

⁸*Shenzhen University, Shenzhen*

⁹*North China Electric Power University, Beijing*

¹⁰*Chinese University of Hong Kong, Hong Kong*

¹¹*Siena College, Loudonville, New York 12211*

¹²*Department of Physics and Astronomy, University of California, Irvine, California 92697*

¹³*University of Science and Technology of China, Hefei*

¹⁴*Charles University, Faculty of Mathematics and Physics, Prague*

¹⁵*Joint Institute for Nuclear Research, Dubna, Moscow Region*

¹⁶*Department of Physics, University of Illinois at Urbana-Champaign, Urbana, Illinois 61801*

¹⁷*Shandong University, Jinan*

¹⁸*Lawrence Berkeley National Laboratory, Berkeley, California 94720*

¹⁹*Department of Physics, Illinois Institute of Technology, Chicago, Illinois 60616*

²⁰*Beijing Normal University, Beijing*

²¹*Department of Nuclear Science and Technology, School of Energy and Power Engineering, Xi'an Jiaotong University, Xi'an*

²²*Wright Laboratory and Department of Physics, Yale University, New Haven, Connecticut 06520*

²³*China Institute of Atomic Energy, Beijing*

²⁴*Guangxi University, No.100 Daxue East Road, Nanning*

²⁵*Center for Neutrino Physics, Virginia Tech, Blacksburg, Virginia 24061*

²⁶*Institute of Physics, National Chiao-Tung University, Hsinchu*

²⁷*Department of Physics, University of Cincinnati, Cincinnati, Ohio 45221*

²⁸*Department of Physics, College of Science and Technology, Temple University, Philadelphia, Pennsylvania 19122*

²⁹*Dongguan University of Technology, Dongguan*

³⁰*Department of Physics, University of California, Berkeley, California 94720*

³¹*Department of Physics, The University of Hong Kong, Pokfulam, Hong Kong*

³²*School of Physics, Nankai University, Tianjin*

³³*Department of Physics and Astronomy, Shanghai Jiao Tong University, Shanghai Laboratory for Particle Physics and Cosmology, Shanghai*

³⁴*Joseph Henry Laboratories, Princeton University, Princeton, New Jersey 08544*

³⁵*The Hong Kong University of Science and Technology, Clear Water Bay, Hong Kong*

³⁶*California Institute of Technology, Pasadena, California 91125*

³⁷*College of William and Mary, Williamsburg, Virginia 23187*

³⁸*Nanjing University, Nanjing*

³⁹*China General Nuclear Power Group, Shenzhen*

⁴⁰*College of Electronic Science and Engineering, National University of Defense Technology, Changsha*

⁴¹*Iowa State University, Ames, Iowa 50011*

⁴²*Chongqing University, Chongqing*

(Dated: October 4, 2022)

Reactor neutrino experiments play a crucial role in advancing our knowledge of neutrinos. A precise measurement of reactor electron antineutrino flux and spectrum evolution can be key inputs in improving the knowledge of neutrino mass and mixing as well as reactor nuclear physics and searching for physics beyond the standard model. In this work, the evolution of the flux and spectrum as a function of the reactor isotopic content is reported in terms of the inverse-beta-decay yield at Daya Bay with 1958 days of data and improved systematic uncertainties. These measurements are compared with two signature model predictions: the Huber-Mueller model based on the conversion method and the SM2018 model based on the summation method. The measured average flux and spectrum, as well as their evolution with the ^{239}Pu isotopic fraction, are inconsistent with the predictions of the Huber-Mueller model. In contrast, the SM2018 model is shown to agree with the average flux and its evolution but fails to describe the energy spectrum. Altering the predicted IBD spectrum from ^{239}Pu fission does not improve the agreement with the measurement for either model. The models can be brought into better agreement with the measurements if either the predicted spectrum due to ^{235}U fission is changed or the predicted ^{235}U , ^{238}U , ^{239}Pu , and ^{241}Pu spectra are changed in equal measure.

PACS numbers: 14.60.Pq, 29.40.Mc, 28.50.Hw, 13.15.+g

Keywords: reactor antineutrino anomaly, sterile neutrino, 5 MeV bump, Huber-Mueller Model, Daya Bay

The detection of reactor electron antineutrinos with the inverse-beta-decay (IBD) process plays a crucial role in advancing our knowledge of neutrinos including the discovery of neutrinos [1], establishment of large mixing angle solution of neutrino oscillation [2], and the discovery of non-zero mixing angle θ_{13} [3]. Looking forward, the JUNO experiment requires an accurate knowledge of the reactor neutrino spectrum to determine the neutrino mass ordering [4].

For commercial reactors, uranium isotopes are introduced at beginning of a fueling cycle and plutonium isotopes are gradually generated. Four fission isotopes ^{235}U , ^{238}U , ^{239}Pu , and ^{241}Pu account for over the 99.7% of the antineutrino flux with energy above the IBD detection threshold [5]. A reactor antineutrino prediction, the Huber-Mueller (HM) model [6, 7], is determined by converting cumulative beta spectra to antineutrino spectra for ^{235}U , ^{239}Pu , and ^{241}Pu and by summing all involved beta decay branches in databases for ^{238}U . The average of reactor neutrino flux measurements is only 95%-96% of the HM prediction, known as the reactor antineutrino anomaly (RAA) [8–11]. Another anomaly is about the spectrum. The measured neutrino spectrum is poorly described by the HM model, e.g. a notable “bump” around 5 MeV [12–14].

Together with other experimental anomalies at short-baseline [15–17], the RAA has motivated a new generation of short-baseline reactor neutrino experiments to search for a sterile neutrino [18–24]. The effect of weak magnetism [25], neutron capture [26], fission-neutron energy [27] and database inaccuracies [28] on the prediction

has been postulated. In particular, approximately 30% of the antineutrino flux comes from forbidden decays which can imply an uncertainty as large as the total flux deficit and the bump [29–33].

Another prediction approach is the summation method, which adds up all related decay branches from databases for all four isotopes. One such example, the SM2018 calculation [34], with the latest experimental inputs, predicted a uniformly lower flux from ^{235}U than the HM model. Kopeikin et al. [35] reported the measured ratio between cumulative β spectra from ^{235}U and ^{239}Pu that is also systematically lower than the HM prediction. Both SM2018 and Kopeikin imply a much smaller discrepancy with neutrino flux measurement than HM.

The most recent results from Daya Bay on the total flux in terms of IBD yield, i.e., the number of antineutrinos per fission multiplied by the IBD cross section [9] and evolution of the spectrum as a function of reactor burnup used a 1230-day data sample [36]. These results showed that the ^{235}U yield is about 8% less than the HM prediction while the ^{239}Pu yield is consistent with the model. The latest total and energy differential yields from ^{235}U and ^{239}Pu with a 1958-day data sample are reported in Ref. [37]. Evolution studies have been performed for the NEOS [38] and RENO [39] experiments.

In this Letter, using the 1958-day data sample taken from December 2011 to August 2017 with the Daya Bay experiment [40], we report the direct measurement of the total and energy differential IBD yields, σ and σ^e , and

their evolution with reactor status with improved systematic uncertainties. Compared to the unfolded spectra of ^{235}U and ^{239}Pu [37], the measurements in this work do not introduce extra uncertainties from the unfolding method and the theoretical uncertainty of ^{238}U and ^{241}Pu which allows a more powerful examination of the combined reactor flux and spectrum prediction of the HM and SM2018 models.

The Daya Bay experiment, equipped with eight antineutrino detectors (ADs), measures the electron antineutrinos from six commercial reactors [41–43]. The results in this Letter are based on approximately 3.5 million IBD candidates detected with the four near-site ADs.

The IBD process, $\bar{\nu}_e + p \rightarrow e^+ + n$, is identified by the prompt-delayed coincidence. The delayed signal corresponds to the neutron captured on gadolinium. The prompt energy, E_p , including the kinetic energy of positron and its annihilation gammas, is related to the antineutrino energy $E_\nu \approx E_p + 0.78$ MeV. The true E_p deposit is reconstructed as E_{rec} . The reconstructed energy resolution is about 8% at 1 MeV and a detector response matrix $M(E_{\text{rec}}, E_\nu)$ is constructed taking into account all detector effects [40]. The measured energy spectrum is corrected for the spent-nuclear-fuel contribution and the nonequilibrium contribution [36, 37] for each AD and week, instead of being treated as time independent in the previous analysis [36].

To measure the IBD yield, a quantity N_i^{dw} is calculated for the d^{th} AD and w^{th} week, and i is 5, 8, 9, and 1 for ^{235}U , ^{238}U , ^{239}Pu , and ^{241}Pu , respectively [5]. It describes the number of fissions of an isotope detected by an AD, and the definition is

$$N_i^{dw} = \sum_{r=1}^{6 \text{ reactors}} \frac{N_d^{\text{Proton}} \bar{P}_{dr}^{\text{sur}} \varepsilon}{4\pi L_{dr}^2} \frac{W_{rw} T_{dw}}{\sum_i f_{irw} e_i} f_{irw}, \quad (1)$$

where N_d^{Proton} is the number of target protons of the d^{th} AD, $\bar{P}_{dr}^{\text{sur}}$ is the average survival probability of reactor electron antineutrinos integrated over energy from the r^{th} reactor to the d^{th} AD calculated under 3-active-neutrino framework in the w^{th} week, ε is the detection efficiency, L_{dr} is the distance of the AD-reactor pair, W_{rw} is the thermal power of the r^{th} reactor for the w^{th} week, which is provided by the reactor company, T_{dw} is the running time of that AD in that week, f_{irw} is the fission fraction of the i^{th} isotope in the r^{th} reactor and w^{th} week, and e_i is the energy per fission of the isotope [44]. The effective fission fraction for the i^{th} isotope, F_i (F_5 , F_8 , F_9 , and F_1), for that AD and week, F_i^{dw} , is defined by $F_i^{dw} \equiv N_i^{dw}/N^{dw}$, in which $N^{dw} = \sum_{i=1}^4 N_i^{dw}$.

Data are sorted into 13 groups according to their effective ^{239}Pu fission fraction F_9^{dw} , which represents the burnup status of reactors and is analogous to the use of F_5^{dw} [36]. In this data set, F_9 ranges from approximately 0.22 to 0.36, and F_5 , correspondingly, ranges from 0.66 to 0.49. The first group corresponds to F_9 between 0.22 and 0.24, due to low statistics, with the additional 12 groups each having a 0.01 interval in F_9 from 0.24 to 0.36. The effective fission fraction of the g^{th} group, F_i^g , is calculated as $F_i^g =$

$\sum_{d,w \in g} N_i^{dw} / \sum_{d,w \in g} N^{dw}$, where the information in each AD and week are added together if their F_9^{dw} 's belong the g^{th} group. The effective fission fractions averaged over all detectors and time (\bar{F}_5 , \bar{F}_8 , \bar{F}_9 , and \bar{F}_1) are (0.564, 0.076, 0.304, and 0.056).

The energy differential IBD yield is measured for six reconstructed energy regions: 0.7-2, 2-3, 3-4, 4-5, 5-6, and 6-8 MeV and the energy differential yield, σ^{eg} , for the e^{th} energy region and the g^{th} fission group is calculated as [5, 36]

$$\sigma^{eg} = \int_e \sum_{d,w \in g} S^{dw}(E_{\text{rec}}) dE_{\text{rec}} / \sum_{d,w \in g} N^{dwe}, \quad (2)$$

where the integral is over the energy region, $S^{dw}(E_{\text{rec}})$ is the measured energy spectrum of the d^{th} AD in the w^{th} week, the divisor gives the total number of fissions for the energy region, and the calculation of N^{dwe} is the same N^{dw} , except that the neutrino survival probability in Eq. 1 is calculated for the e^{th} E_{rec} region only. The sum over e is the total yield, $\sigma^g = \sum_e \sigma^{eg}$, of that group. The evolution of total and energy differential yield with F_9^g are plotted in Fig. 1.

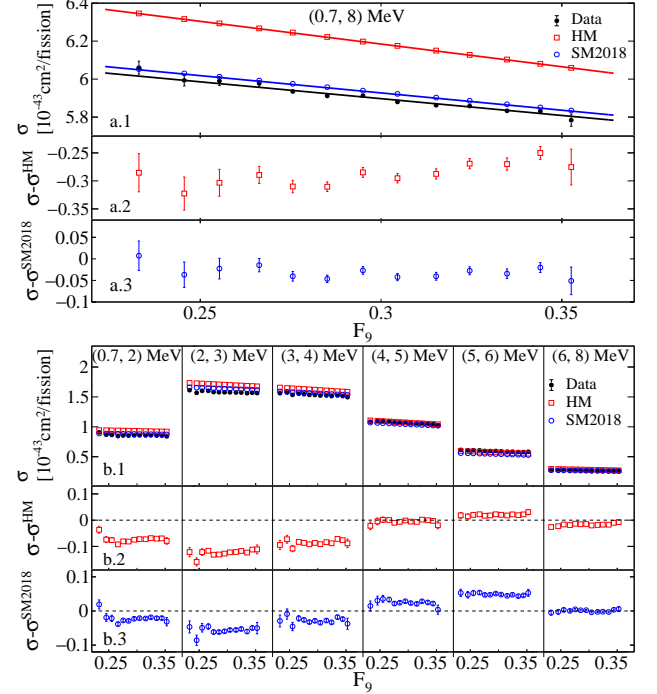


FIG. 1. The panels a.1 and b.1 show the total IBD yields in [0.7, 8] MeV and energy differential yield in six reconstructed energy regions as a function of the effective fission fraction of ^{239}Pu , F_9 , respectively. The best-fit and best-determined lines for the measurements and predictions of the evolution of the total yield are shown in a.1, respectively. The difference between the measurement and the HM and SM2018 predictions for the total yield (a.2 and a.3) and energy differential yields (b.2 and b.3) are also shown. The error bars represent the statistical uncertainties. The units of all panels are $10^{-43} \text{ cm}^2/\text{fission}$.

The uncertainties in σ^g have statistical, background and the following systematic components. For the IBD detection

efficiency, the AD-correlated uncertainty is improved from 1.7% to 0.75% [9], and the AD-uncorrelated uncertainty is 0.11% [37]. The uncertainty of the number of target protons is 0.92% and is AD-correlated [5]. The reactor power measurement uncertainty is 0.5% and is assigned to be reactor-uncorrelated and time-correlated [5]. The uncertainty of the energy per fission is taken into account [44]. The fission fraction uncertainty for the each isotope and reactor is 5%, but the uncertainties of the four isotopes are further constrained with the normalization condition and the correlation matrix [5] and are assigned to be reactor- and time-correlated. The spent nuclear fuel uncertainty is improved from 100% to 30% [40]. The nonequilibrium effect uncertainty is 30% [5]. The θ_{13} -induced oscillation uncertainty is also included [40]. The uncertainty of the energy differential yield of σ^{eg} further includes all the energy spectrum uncertainties from the background shape and detector response [37], in which the uncertainties in the absolute energy scale is reduced to be less than 0.5% for E_{rec} larger than 2 MeV.

The predicted total and energy differential yields of the i^{th} isotope, ($\sigma_5, \sigma_9, \sigma_1,$ and σ_8) and ($\sigma_5^e, \sigma_9^e, \sigma_1^e,$ and σ_8^e) are obtained by convolving the product of model prediction and IBD cross section [5] with the detector response matrix. The total yield predictions is defined as

$$\sigma^{\text{Pred},g} \equiv F_5^g \sigma_5 + F_8^g \sigma_8 + F_9^g \sigma_9 + F_1^g \sigma_1, \quad (3)$$

where σ_i are the yields per isotope. Likewise, using the energy differential predictions, σ_i^e , we define the predicted energy differential yields

$$\sigma^{\text{Pred},eg} \equiv F_5^g \sigma_5^e + F_8^g \sigma_8^e + F_9^g \sigma_9^e + F_1^g \sigma_1^e. \quad (4)$$

The evolution plots of $\sigma^{\text{Pred},g}$ and $\sigma^{\text{Pred},eg}$ with F_9^g are shown in Fig. 1. The differences between the measured and predicted total and energy differential yields are also plotted as a function of F_9^g in Fig. 1.

The uncertainties of $\sigma^{\text{Pred},g}$ and $\sigma^{\text{Pred},eg}$ are from all sources involved in the effective fission fraction calculation as described in Eq. 1, 3 and 4. Model uncertainties are poorly defined and not included unless explicitly stated otherwise.

The total yield evolution is compared to the predictions with two characteristic variables, average yield $\bar{\sigma}$ and normalized evolution slope $(d\sigma/dF_9)/\bar{\sigma}$. The average yield of $\bar{\sigma}$ and slope of $d\sigma/dF_9$ are two direct observables in Fig. 1. The evolution of the predicted yield can be described as a linear function of F_9 for the observed range of F_9 . In addition, if the prediction in Eq. 3 is off by a normalization factor η , for example, induced by large-mass sterile neutrinos [8, 45, 46] or by a global uncertainty, e.g. from the detection efficiency, the prediction would be

$$\sigma^{\text{PredN},g} = \eta(F_5^g \sigma_5 + F_8^g \sigma_8 + F_9^g \sigma_9 + F_1^g \sigma_1). \quad (5)$$

The comparison in the normalized evolution slope $(d\sigma/dF_9)/\bar{\sigma}$ is free of any normalization issue.

The total yield measurements in the 13 fission groups are fitted to the following linear function,

$$\sigma^{\text{Lin},g} = \bar{\sigma} \{1 + [(d\sigma/dF_9)/\bar{\sigma}](F_9^g - \bar{F}_9)\}, \quad (6)$$

with the χ^2 function,

$$\chi^2 = \sum_{gg'} (\sigma^g - \sigma^{\text{Lin},g})(V^{-1})^{gg'} (\sigma^{g'} - \sigma^{\text{Lin},g}), \quad (7)$$

to extract $\bar{\sigma}$ and $(d\sigma/dF_9)/\bar{\sigma}$, where V is a 13×13 covariance matrix determined by randomly sampling all the related uncertainty sources described above. The best-fit results are $\bar{\sigma} = (5.89 \pm 0.07) \times 10^{-43}$ cm²/fission and $[(d\sigma/dF_9)/\bar{\sigma}] = -0.300 \pm 0.024$ with the χ^2 over the number of degrees of freedom, χ^2/NDF , of 9.6/11. The dominant uncertainty of $\bar{\sigma}$ is from the IBD detection efficiency and number of target protons. The dominant uncertainty of $(d\sigma/dF_9)/\bar{\sigma}$ is from statistics. The uncertainties from the effective fission fraction calculation are not significant for them. The best-fit line is shown in Fig. 1, and the results and 68% confidence level contour are shown in Fig. 2.

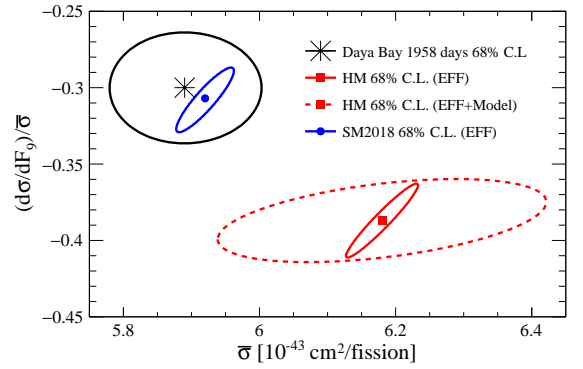


FIG. 2. The measured $\bar{\sigma}$ and $(d\sigma/dF_9)/\bar{\sigma}$ and their 68% confidence level (C.L.) contour is shown. The predictions of the HM and SM2018 models are shown with their 68% C.L. contours with effective fission fraction (EFF) uncertainty. The HM model 68% C.L. contour including its model uncertainties [6, 7] is also shown.

For predictions, $\bar{\sigma}$ and $(d\sigma/dF_9)/\bar{\sigma}$ can be directly calculated for a set of known fission fractions at Daya Bay. A joint distribution of $\bar{\sigma}$ and $(d\sigma/dF_9)/\bar{\sigma}$ is obtained by randomly sampling the effective fission fractions according to their covariance matrix. The mean values and uncertainties of $\bar{\sigma}^{\text{Pred}}$ and $[(d\sigma/dF_9)/\bar{\sigma}]^{\text{Pred}}$ are obtained with the distribution. The results for the HM are $\bar{\sigma}^{\text{HM}} = (6.18 \pm 0.04) \times 10^{-43}$ cm²/fission and $[(d\sigma/dF_9)/\bar{\sigma}]^{\text{HM}} = -0.387 \pm 0.016$ ($(6.18 \pm 0.16) \times 10^{-43}$ cm²/fission and -0.387 ± 0.018 if including the model uncertainties [6, 7]). The HM prediction in $\bar{\sigma}$ and $(d\sigma/dF_9)/\bar{\sigma}$ are rejected at 3.6 and 3.0 standard deviations. For SM2018, the results are consistent with the Daya Bay measurements. These results are shown in Fig. 2 and the best-determined lines are plotted in Fig. 1.

The energy differential yield evolution is compared to models with the average yields and normalized evolution

slopes in six reconstructed energy regions. The data are simultaneously fitted to six linear functions,

$$\sigma^{\text{Lin}, eg} = \bar{\sigma}^e \{1 + [(d\sigma/dF_9)/\bar{\sigma}]^e (F_9^g - \bar{F}_9)\}, \quad (8)$$

with the χ^2 function,

$$\chi^2 = \sum_{ege'g'} (\sigma^{eg} - \sigma^{\text{Lin}, eg})(U^{-1})^{ege'g'} (\sigma^{e'g'} - \sigma^{\text{Lin}, e'g'}), \quad (9)$$

to extract six pairs of parameters of $\bar{\sigma}^e$ and $[(d\sigma/dF_9)/\bar{\sigma}]^e$, where U is a 78×78 covariance matrix with a combined row (column) index of eg ($e'g'$) for the e^{th} (e'^{th}) reconstructed energy region and g^{th} (g'^{th}) fission fraction group. U is also determined by a random sampling method of all the related uncertainty sources described earlier. The best-fit χ^2/NDF is 76/66. The fit also gives the 12×12 covariance matrix of $\bar{\sigma}_e$ and $[(d\sigma/dF_9)/\bar{\sigma}]^e$, which includes the 6×6 covariance matrix, A , for the six $\bar{\sigma}^e$ and the 6×6 covariance matrix, B , for $[(d\sigma/dF_9)/\bar{\sigma}]^e$. The six $\bar{\sigma}^e$ results are strongly correlated because their dominant uncertainties are from the IBD detection efficiency and number of target protons, and the matrix A deviates strongly from a diagonal matrix. The six $[(d\sigma/dF_9)/\bar{\sigma}]^e$ results are all limited by data statistics and largely uncorrelated, and B is close to diagonal. The correlation between $\bar{\sigma}^e$ and $[(d\sigma/dF_9)/\bar{\sigma}]^e$ is insignificant.

For the predictions, a joint 12-dimension distribution of $\bar{\sigma}^e$ and $[(d\sigma/dF_9)/\bar{\sigma}]^e$ is obtained by randomly sampling the effective fission fractions as for the study of the predicted total yield and its normalized evolution rate. The mean values of $\bar{\sigma}^{\text{Pred}, e}$ and $[(d\sigma/dF_9)/\bar{\sigma}]^{\text{Pred}, e}$ are obtained with the distribution as well as the covariance matrix for $\bar{\sigma}^{\text{Pred}, e}$, A^{Pred} , and the covariance matrix for $[(d\sigma/dF_9)/\bar{\sigma}]^{\text{Pred}, e}$, B^{Pred} . The difference of $\bar{\sigma}^{\text{Pred}, e}$ with the measurement and $[(d\sigma/dF_9)/\bar{\sigma}]^{\text{Pred}, e}$ results are plotted in Fig. 3. The uncertainty associated with prediction is much smaller than that from measurement.

The average IBD yields of six energy regions, $\bar{\sigma}^e$ are compared to the HM and SM2018 predictions $\bar{\sigma}^{\text{Pred}, e}$. Their difference is quantified as a χ^2 calculated with the difference of $\bar{\sigma}^e - \bar{\sigma}^{\text{Pred}, e}$ and their covariance matrix of $A + A^{\text{Pred}}$. The resulting χ^2/NDF and the corresponding extent of discrepancy in standard deviations are shown in Tab. I. The models do not agree with Daya Bay, and because of the deficit around 3 MeV and/or the bump around 5 MeV found in the measurement (Fig. 1) and the strong correlation among the measurements in different energy regions, their χ^2/NDF 's are rather large, and they correspond to 25 and 27 standard deviations for the HM and SM2018 models, respectively. The latter, due to the larger discrepancy in the 4-6 MeV region with the measurement, has a slightly worse χ^2/NDF than HM.

The normalized evolution slopes of the six energy regions, $[(d\sigma/dF_9)/\bar{\sigma}]^e$, are compared to HM and SM2018. Their difference is quantified with a χ^2 calculated with the difference of $[(d\sigma/dF_9)/\bar{\sigma}]^e - [(d\sigma/dF_9)/\bar{\sigma}]^{\text{Pred}, e}$ and their covariance matrix of $B + B^{\text{Pred}}$. The resulting χ^2/NDF is shown in Tab. I. While the HM and SM2018 models poorly

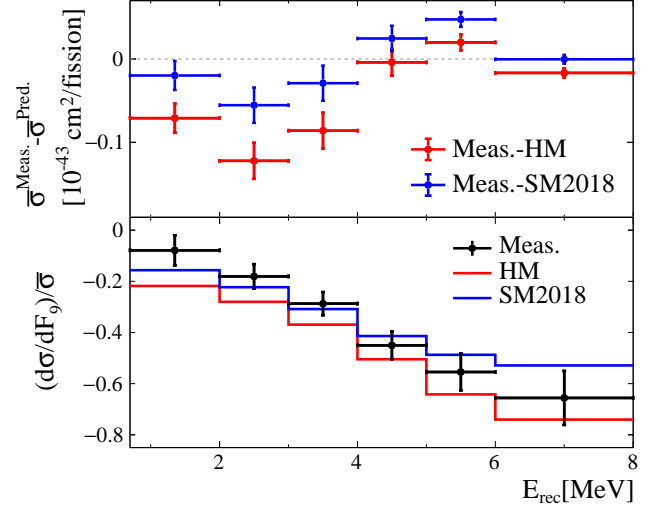


FIG. 3. The upper panel shows the difference between the measured energy differential yields and predictions for six reconstructed energy bins, where the error bars are from the measurement. The lower panel shows the normalized evolution slopes for the measurement and predictions, where the uncertainties of measurement are shown.

TABLE I. Comparison results of the measurement with the HM and SM2018 predictions for the average IBD yields of six energy regions, $\bar{\sigma}^e$, (middle column) and the normalized evolution slopes, $[(d\sigma/dF_9)/\bar{\sigma}]^e$ (right column). The χ^2/NDF of the comparison (corresponding number of standard deviations) is given.

Model	$\bar{\sigma}^e$	$[(d\sigma/dF_9)/\bar{\sigma}]^e$
HM	675/6 (25)	11/6 (1.8)
SM2018	748/6 (27)	5.5/6 (0.7)

predict the spectral shape, their predicted relative changes with the fuel composition have much better agreement with the measurement.

To understand the difference between the Daya Bay differential IBD yield evolution and the predictions, three types of modified models with new free parameters are introduced on top of the HM and SM2018 predictions.

The first modification to each model is to alter only the ^{235}U energy differential yield prediction in each reconstructed energy region by the fraction f_5^e together with the global normalization factor η , as in Eq. 5,

$$\sigma^{\text{model}, eg} = \eta [F_5^g \sigma_5^e (1 + f_5^e) + F_8^g \sigma_8^e + F_9^g \sigma_9^e + F_1^g \sigma_1^e]. \quad (10)$$

Depending on what the base model is, the modified models are further labelled as HM+ ^{235}U and SM2018+ ^{235}U . This is motivated by the fact that the majority of the the neutrino flux is due to ^{235}U .

In the second modification to each model, the prediction is

$$\sigma^{\text{model},eg} = \eta[F_5^g \sigma_5^e + F_8^g \sigma_8^e + F_9^g \sigma_9^e(1 + f_9^e) + F_1^g \sigma_1^e], \quad (11)$$

where only the ^{239}Pu energy differential yield predictions in each reconstructed energy region is allowed to change by the fraction f_9^e together with the global normalization factor η . The modified models are labelled as HM+ ^{239}Pu and SM2018+ ^{239}Pu next. This is motivated given that ^{239}Pu is the second largest contributor to the neutrino flux.

The third modification to each model is to equally scale the predicted spectra of four isotopes in each reconstructed energy region by the fraction f_E^e ,

$$\sigma^{\text{model},eg} = (1 + f_E^e)[F_5^g \sigma_5^e + F_8^g \sigma_8^e + F_9^g \sigma_9^e + F_1^g \sigma_1^e]. \quad (12)$$

The motivation is that particular studies [30, 47] have suggested that all four isotopes may have a common problem in predictions. They are labelled as HM+Equ and SM2018+Equ.

We fit the measured energy differential yields in the 6 energy regions and 13 fission fraction groups to the modified models with the following χ^2

$$\chi^2 = \sum_{ege'g'} (\sigma^{eg} - \sigma^{\text{model},eg})(Q^{-1})^{ege'g'} (\sigma^{e'g'} - \sigma^{\text{model},e'g'}), \quad (13)$$

where six f_e 's and/or η are free parameters and Q is a 78×78 covariance matrix including all uncertainties for the measurement and predictions determined as V of Eq. 7 or U of Eq. 9. When using Eq. 10 or Eq. 11, fits are also performed with η fixed to 1. The best-fit χ^2/NDF , the corresponding extent of discrepancy in standard deviations, and best-fit η , when applicable, are shown in Tab. II. The best-fit f_5^e and f_9^e of Eq. 10 and Eq. 11 with η fixed to 1, and f_E^e in Eq. 12 are shown in Fig. 4. The difference of the deduced $\bar{\sigma}^{\text{model},e}$ with measurement and the deduced $[(d\sigma/dF_9)/\bar{\sigma}]^{\text{model},e}$ are also shown in the figure, and where the first and third model modifications are preferred with respect to the second model.

Even when the ^{239}Pu energy spectra are modified, both the HM and SM2018 model predictions remain incompatible with the data at well over three standard deviations as shown in Tab. II. For both models, as seen in Fig. 4, the required changes of the ^{239}Pu spectrum in some regions are higher than 40%, which is far beyond the range of uncertainties caused by the various postulated mechanisms [25–33] and is unreasonable. This observation can be phenomenologically traced back to the features of Fig. 1. For example, the $\bar{\sigma}^e - \bar{\sigma}^{\text{HM},e}$ in the 2-4 MeV region shows a positive slope and is not proportional to F_9 , which contradicts the assumption of pure ^{239}Pu -caused anomaly [38, 39].

The attempts to adjust the predicted spectrum of ^{235}U or all spectra in equal measure all lead to good agreement with the data using this metric. As shown in Tab. II, their best-fit η results for ^{235}U -adjusting models are all consistent with 1.

TABLE II. For the six modified models in Eq. 10, 11, and 12 (the first column), the best-fit χ^2/NDF when fitting to data and the corresponding number of standard deviations are shown in the second column and the determined normalization factor η in the third column. Trials are also done with η fixed to 1 for Eq. 10 and Eq. 11.

Model	χ^2/NDF	η
HM+ ^{235}U	83/71 (1.4)	0.985±0.021
	83/72 (1.4)	1 (fixed)
SM2018+ ^{235}U	80/71 (1.2)	0.997±0.021
	80/72 (1.2)	1 (fixed)
HM+ ^{239}Pu	116/71 (3.4)	0.935±0.014
	136/72 (4.5)	1 (fixed)
SM2018+ ^{239}Pu	126/71 (4.0)	0.995±0.014
	127/72 (4.0)	1 (fixed)
HM+Equ	89/72 (1.7)	NA
SM2018+Equ	82/72 (1.3)	NA

The deduced $\bar{\sigma}^{\text{model},e}$ and $[(d\sigma/dF_9)/\bar{\sigma}]^{\text{model},e}$ are consistent with the measurements as shown in Fig. 4. HM+ ^{235}U works slightly better than HM+Equ model, as their best-fit χ^2/NDF shown in Tab. II. But with the current precision of the Daya Bay data set, it is difficult to distinguish whether ^{235}U , by itself, or a mix of fission isotopes, are responsible for the flux and spectrum anomalies.

In summary, the total and energy differential IBD yield evolution as a function of fuel composition are measured and compared to the predictions of two signature models: the HM model based on the conversion method and the SM2018 model based on the summation method. While the measurement of the total IBD yield evolution is found to be incompatible with the HM model prediction, it is consistent with the SM2018 prediction. On the other hand, the predictions of spectrum evolution for both HM and SM2018 model show large discrepancies from the data. We exclude at high significance the hypothesis that the ^{239}Pu energy spectrum in HM or SM2018 models is responsible for the entire difference with the data, regardless of how the normalization of the Daya Bay data is treated. In contrast, good consistency with the data can be achieved either by altering the ^{235}U spectrum or all four isotopes' spectra in equal measure in the SM2018 model. For the HM model, the ^{235}U spectrum adjustment works slightly better than adjusting all spectra, as indicated by the total yield evolution measurement. Future enhancements to the models could prioritize ^{235}U -specific causes or factors common to the four isotopes.

Daya Bay is supported in part by the Ministry of Science and Technology of China, the U.S. Department of Energy, the Chinese Academy of Sciences, the National Natural Science Foundation of China, the Guangdong provincial government, the Shenzhen municipal government, the China General Nuclear Power Group, Key Laboratory of Particle and Radiation Imaging (Tsinghua University), the Ministry of Education, Key Laboratory of Particle

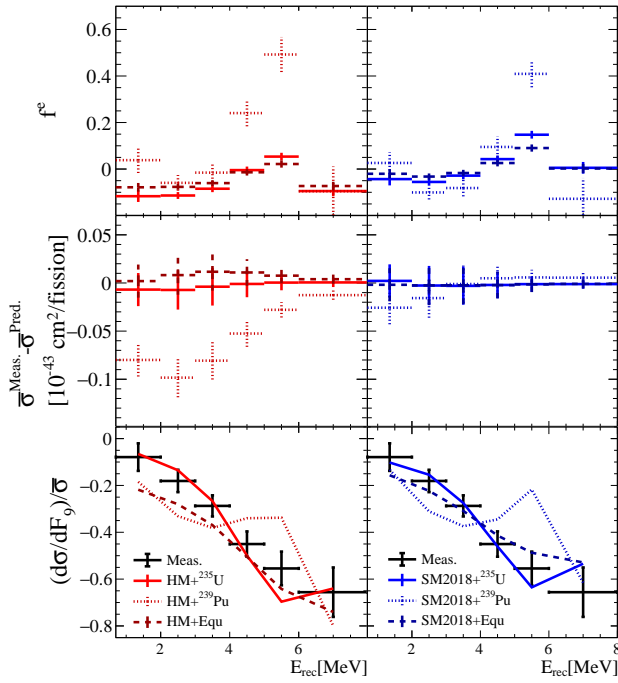


FIG. 4. The best-fit f^e , i.e. f_5^e , f_9^e or f_E^e , values of the modified models of $\text{HM}+^{235}\text{U}$, $\text{SM2018}+^{235}\text{U}$ (Eq. 10 with η fixed to 1), $\text{HM}+^{239}\text{Pu}$, $\text{SM2018}+^{239}\text{Pu}$ (Eq. 11 with η fixed to 1), $\text{HM}+\text{Equ}$, and $\text{SM2018}+\text{Equ}$ (Eq. 12) are shown in the upper panels, where the error bars are fit results. The deduced $\bar{\sigma}^{\text{model},e}$ predictions with the corresponding f^e values for each model are shown as the difference with the measurement in the middle panels and the error bars shown are from the measurement. The measured $[(d\sigma/dF_9)/\bar{\sigma}]^e$ and deduced $[(d\sigma/dF_9)/\bar{\sigma}]^{\text{model},e}$ are shown in the lower panels and only the error bars of measurement are shown.

Physics and Particle Irradiation (Shandong University), the Ministry of Education, Shanghai Laboratory for Particle Physics and Cosmology, the Research Grants Council of the Hong Kong Special Administrative Region of China, the University Development Fund of The University of Hong Kong, the MOE program for Research of Excellence at National Taiwan University, National Chiao-Tung University, and NSC fund support from Taiwan, the U.S. National Science Foundation, the Alfred P. Sloan Foundation, the Charles University Research Center UNCE/SCI/013 in the Czech Republic, the Joint Institute of Nuclear Research in Dubna, Russia, the CNFC-RFBR joint research program, the National Commission of Scientific and Technological Research of Chile, and the Tsinghua University Initiative Scientific Research Program. We acknowledge Yellow River Engineering Consulting Co., Ltd., and China Railway 15th Bureau Group Co., Ltd., for building the underground laboratory. We are grateful for the ongoing cooperation from the China General Nuclear Power Group and China Light and Power Company.

- * Now at Department of Chemistry and Chemical Technology, Bronx Community College, Bronx, New York 10453
† Now at Department of Physics and Astronomy, University of Rochester, Rochester, New York 14627
‡ Now at Department of Physics and Astronomy, Louisiana State University, Baton Rouge, LA 70803
- [1] F. Reines and C. L. Cowan, *Nature* **178**, 446 (1956).
 - [2] K. Eguchi *et al.* (KamLAND), *Phys. Rev. Lett.* **90**, 021802 (2003).
 - [3] F. P. An *et al.* (Daya Bay), *Phys. Rev. Lett.* **108**, 171803 (2012).
 - [4] F. An *et al.* (JUNO), *J. Phys. G* **43**, 030401 (2016).
 - [5] F. P. An *et al.* (Daya Bay), *Chin. Phys. C* **41**, 013002 (2017).
 - [6] P. Huber, *Phys. Rev. C* **84**, 024617 (2011).
 - [7] T. A. Mueller *et al.*, *Phys. Rev. C* **83**, 054615 (2011).
 - [8] G. Mention *et al.*, *Phys. Rev. D* **83**, 073006 (2011).
 - [9] D. Adey *et al.* (Daya Bay), *Phys. Rev. D* **100**, 052004 (2019).
 - [10] S. G. Yoon *et al.* (RENO), *Phys. Rev. D* **104**, L111301 (2021).
 - [11] H. de Kerret *et al.* (Double Chooz), *Nature Phys.* **16**, 558 (2020).
 - [12] F. P. An *et al.* (Daya Bay), *Phys. Rev. Lett.* **116**, 061801 (2016).
 - [13] J. H. Choi *et al.* (RENO), *Phys. Rev. Lett.* **116**, 211801 (2016).
 - [14] Y. Abe *et al.* (Double Chooz), *JHEP* **10**, 086 (2014).
 - [15] A. Aguilar-Arevalo *et al.* (LSND), *Phys. Rev. D* **64**, 112007 (2001).
 - [16] A. A. Aguilar-Arevalo *et al.* (MiniBooNE), *Phys. Rev. Lett.* **105**, 181801 (2010).
 - [17] P. Anselmann *et al.* (GALLEX), *Phys. Lett. B* **342**, 440 (1995).
 - [18] I. Alekseev *et al.*, *Physics Letters B* **787**, 56 (2018).
 - [19] Y. J. Ko *et al.* (NEOS Collaboration), *Phys. Rev. Lett.* **118**, 121802 (2017).
 - [20] A. Serebrov *et al.* (NEUTRINO-4), *Pisma Zh. Eksp. Teor. Fiz.* **109**, 209 (2019).
 - [21] M. Andriamirado *et al.* (PROSPECT), (2020), arXiv:2006.11210 [hep-ex].
 - [22] Y. Abreu *et al.* (SoLid), *JINST* **14**, P11003 (2019).
 - [23] H. Almazán *et al.* (STEREO), *J. Phys. G* **48**, 075107 (2021).
 - [24] V. V. Barinov *et al.*, *Phys. Rev. Lett.* **128**, 232501 (2022).
 - [25] X. B. Wang and A. C. Hayes, *Phys. Rev. C* **95**, 064313 (2017).
 - [26] P. Huber and P. Jaffke, *Phys. Rev. Lett.* **116**, 122503 (2016).
 - [27] B. R. Littlejohn, A. Conant, D. A. Dwyer, A. Erickson, I. Gustafson, and K. Hermanek, *Phys. Rev. D* **97**, 073007 (2018).
 - [28] A. C. Hayes, J. L. Friar, G. T. Garvey, D. Ibeling, G. Jungman, T. Kawano, and R. W. Mills, *Phys. Rev. D* **92**, 033015 (2015).
 - [29] A. C. Hayes, J. L. Friar, G. T. Garvey, G. Jungman, and G. Jonkmans, *Phys. Rev. Lett.* **112**, 202501 (2014).
 - [30] L. Hayen, J. Kostensalo, N. Severijns, and J. Suhonen, *Phys. Rev. C* **100**, 054323 (2019).
 - [31] Y.-F. Li and D. Zhang, *Phys. Rev. D* **100**, 053005 (2019).
 - [32] D.-L. Fang and B. A. Brown, *Phys. Rev. C* **91**, 025503 (2015).
 - [33] A. A. Sonzogni, T. D. Johnson, and E. A. McCutchan, *Phys. Rev. C* **91**, 011301 (2015).
 - [34] M. Estienne *et al.*, *Phys. Rev. Lett.* **123**, 022502 (2019).
 - [35] V. Kopeikin, M. Skorokhvatov, and O. Titov, *Phys. Rev. D* **104**, L071301 (2021).
 - [36] F. P. An *et al.* (Daya Bay), *Phys. Rev. Lett.* **118**, 251801 (2017).
 - [37] D. Adey *et al.* (Daya Bay), *Phys. Rev. Lett.* **123**, 111801 (2019).
 - [38] P. Huber, *Phys. Rev. Lett.* **118**, 042502 (2017).
 - [39] G. Bak *et al.* (RENO), *Phys. Rev. Lett.* **122**, 232501 (2019).
 - [40] D. Adey *et al.* (Daya Bay), *Phys. Rev. Lett.* **121**, 241805 (2018).
 - [41] D. Adey *et al.* (Daya Bay), *Phys. Rev. Lett.* **121**, 241805 (2018).

- [42] F. P. An *et al.* (Daya Bay), Phys. Rev. D **93**, 072011 (2016).
- [43] F. An *et al.* (Daya Bay), Phys. Rev. D **95**, 072006 (2017).
- [44] X. B. Ma, W. L. Zhong, L. Z. Wang, Y. X. Chen, and J. Cao, Phys. Rev. C **88**, 014605 (2013).
- [45] F. P. An *et al.* (Daya Bay), Phys. Rev. Lett. **113**, 141802 (2014).
- [46] A. Palazzo, JHEP **10**, 172 (2013).
- [47] M. Xubo, Y. Le, Z. Liang, A. Fengpeng, and C. Jun, (2018), arXiv:1807.09265 [nucl-ex].